Organic & Biomolecular Chemistry

Cite this: *Org. Biomol. Chem.*, 2011, **9**, 5845

www.rsc.org/obc

PAPER

Theoretical studies on the mechanism and stereoselectivity of Rh(Phebox)-catalyzed asymmetric reductive aldol reaction†

Yun-Fang Yang,[a] Ting Shi,[a,b] Xin-Hao Zhang,[a] Zong-Xun Tang,[b] Zhen-Yi Wen,[b] Jun-Min Quan[a] and Yun-Dong Wu*[a,c,d]

Received 31st March 2011, Accepted 23rd May 2011
DOI: 10.1039/c1ob05501a

Density functional theory calculations (B3LYP) have been carried out to understand the mechanism and stereochemistry of an asymmetric reductive aldol reaction of benzaldehyde and *tert*-butyl acrylate with hydrosilanes catalyzed by Rh(Phebox-ip)$(OAc)_2(OH_2)$. According to the calculations, the reaction proceeds *via* five steps: (1) oxidative addition of hydrosilane, (2) hydride migration to carbon–carbon double bond of *tert*-butyl acrylate, which determines the chirality at C2, (3) tautomerization from rhodium bound C-enolate to rhodium bound O-enolate, (4) intramolecular aldol reaction, which determines the chirality at C3 and consequently the *anti*/*syn*-selectivity, and (5) reductive elimination to release aldol product. The hydride migration is the rate-determining step with a calculated activation energy of 23.3 kcal mol^{-1}. In good agreement with experimental results, the formation of *anti*-aldolates is found to be the most favorable pathway. The observed *Si*-facial selectivity in both hydride migration and aldol reaction are well-rationalized by analyzing crucial transition structures. The *Re*-facial attack transition state is disfavored because of steric hindrance between the isopropyl group of the catalyst and the *tert*-butyl acrylate.

Introduction

Chiral Lewis acid-catalyzed asymmetric reductive aldol reaction is one of the most important and valuable reactions in organic synthesis[1] and has been the subject of extensive studies.[2] However, to fully understand the reaction mechanism and the origin of stereochemistry is still a major challenge for experimentalists as well as theoreticians.

Reductive aldol reactions proceed *via* two key steps, metal-mediated conjugate addition[3] and intramolecular aldol reaction between the metal enolate and aldehyde. As valuable synthetic tools for complex ketones and carboxylic acid derivatives, metal-catalyzed aldol reactions between aldehydes and α,β-unsaturated esters or enones have been widely investigated.[4] Following the first rhodium-catalyzed intermolecular reductive aldol reaction demonstrated by Revis and Hilty in 1987,[5] a large number of related studies with different metals have been described.[6] In these reactions, reducing reagents such as silane derivatives or hydrogen gas were introduced as the terminal reductant, and different diastereo- and enantio-selectivities were delivered. In 2004, Morken *et al.* and Shibata *et al.* reported two catalyzed reactions attaining asymmetric induction accompanied by *syn*-diastereoselectivity by using chiral phosphine-rhodium and di-haloindium hydride catalysts, respectively.[7] Good diastereoselectivity in favor of the *syn* isomer in nickel-catalyzed reductive aldol reactions was also explored by Christa and John in 2007.[8] However, enantioselective *anti*-aldol reactions are rare.

Nishiyama reported a chiral 2,6-bis(2-oxazolinyl)phenyl skeleton (abbreviated as Phebox) N–C–N ligand and some of its transition metal complexes, which were expected to exhibit high potential as Lewis acids in asymmetric reactions.[9] Furthermore, experiments with catalytic amounts of Rh(Phebox) complexes for the asymmetric conjugate reaction of α,β-unsaturated esters with aldehydes and several hydrosilanes have been demonstrated.[10] The *anti* isomers have been selectively obtained in the ratio of 94 : 6–95 : 5 with high enantioselectivity up to 96% ee (Scheme 1). By some control experiments, Nishiyama and coworkers confirmed that the aldol reaction took place on the rhodium center and the stereochemistry was determined by the chiral catalyst.[10] Based on the outcome of *anti*-isomers and some preliminary modeling of hypothetical intermediates, they proposed a plausible chair-like transition state which might be responsible for the facial selectivity. However, detailed mechanistic information and the origin of stereoselectivity remained unknown.

To rationalize the experimental observations and to design new catalytic systems, a deeper understanding of the reaction processes for the rhodium-catalyzed aldol reaction at a molecular

[a]*School of Chemical Biology and Biotechnology, Shenzhen Graduate School of Peking University, Shenzhen 518055, China*
[b]*Department of Chemistry, Northwest University, Xi'an 710069, China*
[c]*Department of Chemistry, The Hong Kong University of Science & Technology, Clear Water Bay, Kowloon, Hong Kong, China. E-mail: chydwu@ust.hk*
[d]*College of Chemistry, Peking University, Beijing 100871, China*

† Electronic supplementary information (ESI) available: Cartesian coordinates for all transition state structures along the interconversion pathways. See DOI: 10.1039/c1ob05501a

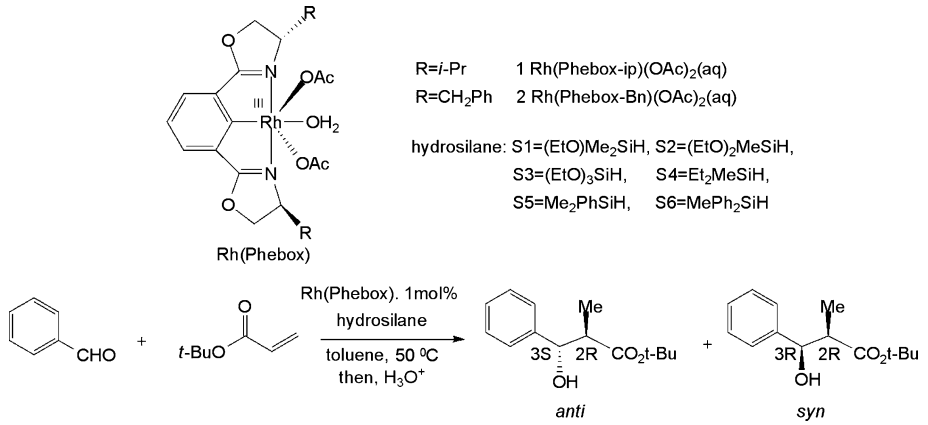

Scheme 1 Asymmetric reductive aldol reaction of *tert*-butyl acrylate and benzaldehyde with Rh(Phebox) catalysts.

level is necessary, for which the present computational chemistry is well-suited.[11] In this paper we aim to address the following questions: (1) what is the detailed mechanism, *i.e.* elementary steps of favorable pathways, of the Rh(Phebox-ip)-catalyzed asymmetric reductive aldol reaction? (2) what is the origin of stereoselectivity, *i.e.* regio- and diastereo-selectivity?

The computational method

All calculations have been carried out with the Gaussian 03 program.[12] Geometries of all the stationary points were fully optimized by the B3LYP method,[13] and the nature of these structures was verified by harmonic vibrational frequency analysis. Minima were characterized by all real frequencies, while transition states have one and only one imaginary frequency. In these calculations, the 6-31G(d) basis set[14] was used for H, C, N and O atoms, while the Lanl2dz basis set[15] was used for Si and Rh atoms. Intrinsic reaction coordinates (IRC)[16] calculations were performed to confirm that transition state structures indeed connect two relevant minima. To evaluate solvent effect, single-point energy calculations with the self-consistent reaction field (SCRF) calculation based on the polarizable continuum model (PCM,[17] $\varepsilon = 2.247$ for toluene, which is used as the solvent in experiments) were carried out at the same level as the one used for geometry optimization.

Results and discussion

1 Structure analysis of the Rh(Phebox-ip)$(OAc)_2(OH_2)$ complex

The molecular structure of the catalyst (Rh(Phebox-ip)$(OAc)_2$-(OH_2)) was analyzed by X-ray crystallography (CCDC-248010) and showed a C_2 symmetric form.[18] Our calculation on the structure of the catalyst gives rather reliable values compared to the bond lengths and bond angle of the X-ray structure (Table 1). As shown in Fig. 1, the catalyst Rh(Phebox-ip)$(OAc)_2(OH_2)$ is a 6-coordinated complex with an N–C–N pincer ligand, two axial AcO ligands and a neutral water ligand. Hydrogen-bonding was found between the metal-bound water and the axial AcO ligands. Once the catalyst goes into the catalytic cycle, it is a necessity that the water ligand dissociates to afford vacant sites which can recruit substrates. It is proposed by Nishiyama that the starting Rh^{III} complex can be reduced by an excess of hydrosilane to form Rh^{I} species, which reacts with hydrosilane again to give an H–Rh^{III}–Si active species as the catalyst.[10] So the catalyst (Rh^{III}(Phebox-ip)$(OAc)_2(OH_2)$) can be regarded as a precatalyst and the (Rh^{I}(Phebox-ip)) complex is considered as the active catalyst.

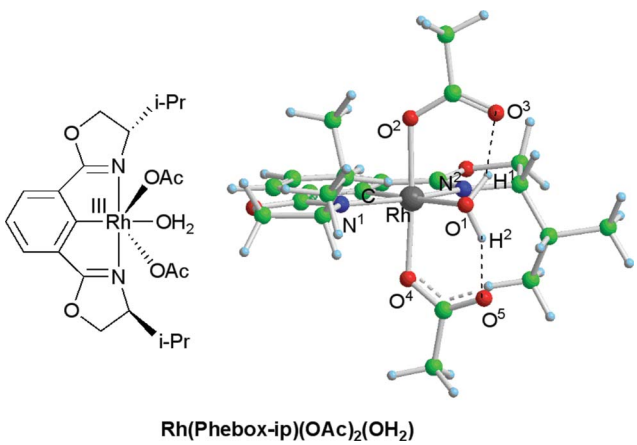

Fig. 1 Structure of the catalyst Rh(Phebox-ip)$(OAc)_2(OH_2)$.

Table 1 Selected bond lengths and bond angle of the catalyst Rh(Phebox-ip)$(OAc)_2(OH_2)$

	Bond length [Å]								Bond angle [°]
	Rh–C	Rh–N^1	Rh–N^2	Rh–O^1	Rh–O^2	Rh–O^4	O^1–O^3	O^1–O^5	N^1–Rh–N^2
Crystal Structure	1.924	2.058	2.088	2.232	2.026	2.047	2.673	2.601	158.358
Calculation	1.945	2.098	2.125	2.259	2.075	2.080	2.689	2.644	157.955

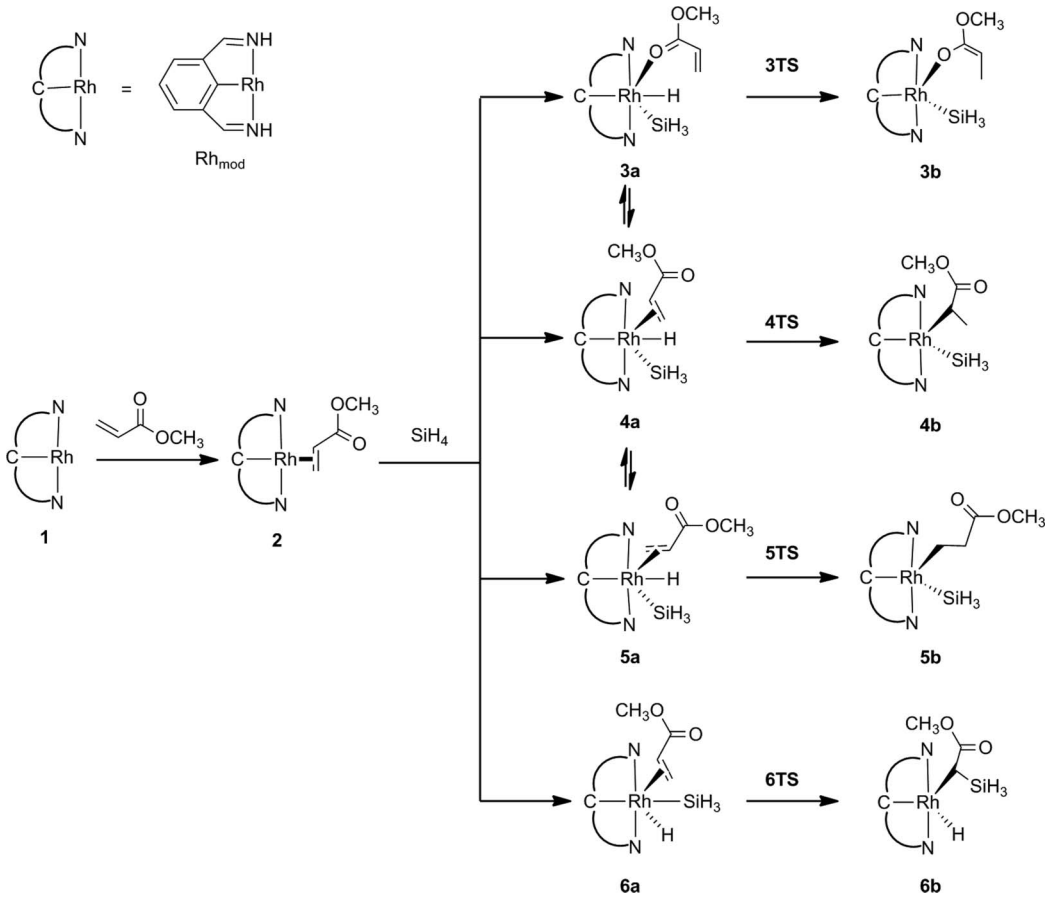

Scheme 2 Si–H oxidative addition and hydride/silyl migration with simplified model system.

2 Calculations of model species

Based on the experimental findings, Nishiyama and co-workers proposed the reaction sequence as: the starting Rh^{III}(Phebox) reacts with hydrosilane *via* a Rh^{I} complex to give a Rh^{III} hydride; the hydride then migrates into α,β-unsaturated ester to produce Rh^{III} enolate, which couples with benzaldehyde; the final aldol product is released by a reductive elimination step. However, for such a complicated reaction which involves four components, *i.e.* Rh catalyst, hydrosilane, α,β-unsaturated ester and aldehyde, what is the reaction process in detail? Is there any other alternative pathway? It is more reasonable to use a simplified model for a preliminary exploration to identify the most favorable pathway. As shown in Scheme 2, model complex **1** (Rh_{mod}), SiH_4, and methyl acrylate were chosen to mimic the structural and electronic features of Rh^{I}(Phebox-ip), hydrosilane and α,β-unsaturated ester, respectively. Based on the Chalk–Harrod mechanism and the modified Chalk–Harrod mechanism proposed for the metal-catalyzed hydrosilylation,[19] four possible pathways were suggested as shown in Scheme 2.

The carbon–carbon double bond (C═C) of methyl acrylate coordinates to Rh_{mod} **1** producing complex **2**. Following the oxidative addition of SiH_4 to complex **2**, four isomers can be directly obtained through optimizations. In **3a**, methyl acrylate coordinates to the Rh center with the oxygen atom of the carbonyl, while in **4a**, **5a** and **6a**, methyl acrylate coordinates to the Rh center with its vinyl group. Due to the lack of strong π back donation, Rh–carbonyl complex **3a** lies *ca.* 6 kcal mol^{-1} higher than those Rh-vinyl complexes **4a**, **5a**, and **6a**. The optimized geometries show that the H atom is located on the Phebox plane in **4a** and **5a**, and the C═C double bond is parallel to the Rh–H bond. Different orientations of methyl acrylate in **4a** and **5a** cause only a negligible energy difference. In terms of regioselectivity for hydride migration, the hydride may either migrate to the acrylate β-carbon in **4a** or migrate to the acrylate α-carbon in **5a**. In contrast to the others, **6a** adopts a structure where the SiH_3 group is on the Phebox plane and the C═C bond is *trans* to the hydride. Due to the stronger *trans* influence of SiH_3 than that of H,[20] **6a** is less stable than **4a** by about 1.2 kcal mol^{-1}.

Transition states leading to a migration have been located and denoted as **3TS**, **4TS**, **5TS** and **6TS**, respectively (Fig. 2). **3TS** is a twisted six-membered ring transition state for 1,4-addition, while **4TS**, **5TS** and **6TS** are four-membered-ring transition states for 1,2-addition. The calculated relative free energies indicate that the Rh-bound C═C is more reactive than the unbound C═C group of methyl acrylate, and the hydride migration is more favorable than the silyl migration. **3TS** is less stable than **4TS** by 18.0 kcal mol^{-1}. The calculated activation energy of hydride migration to acrylate β-carbon is about 17.3 kcal mol^{-1} and identical to the result (17.3 kcal mol^{-1}) reported by Sakaki *et al.*[21] **4TS** is the most stable transition state among these four. The barrier for hydride migration to the acrylate α-carbon (**5TS**) is *ca.* 3.5 kcal mol^{-1} higher than that to the acrylate β-carbon (**4TS**). It is understandable because the β-carbon is supposed to carry more

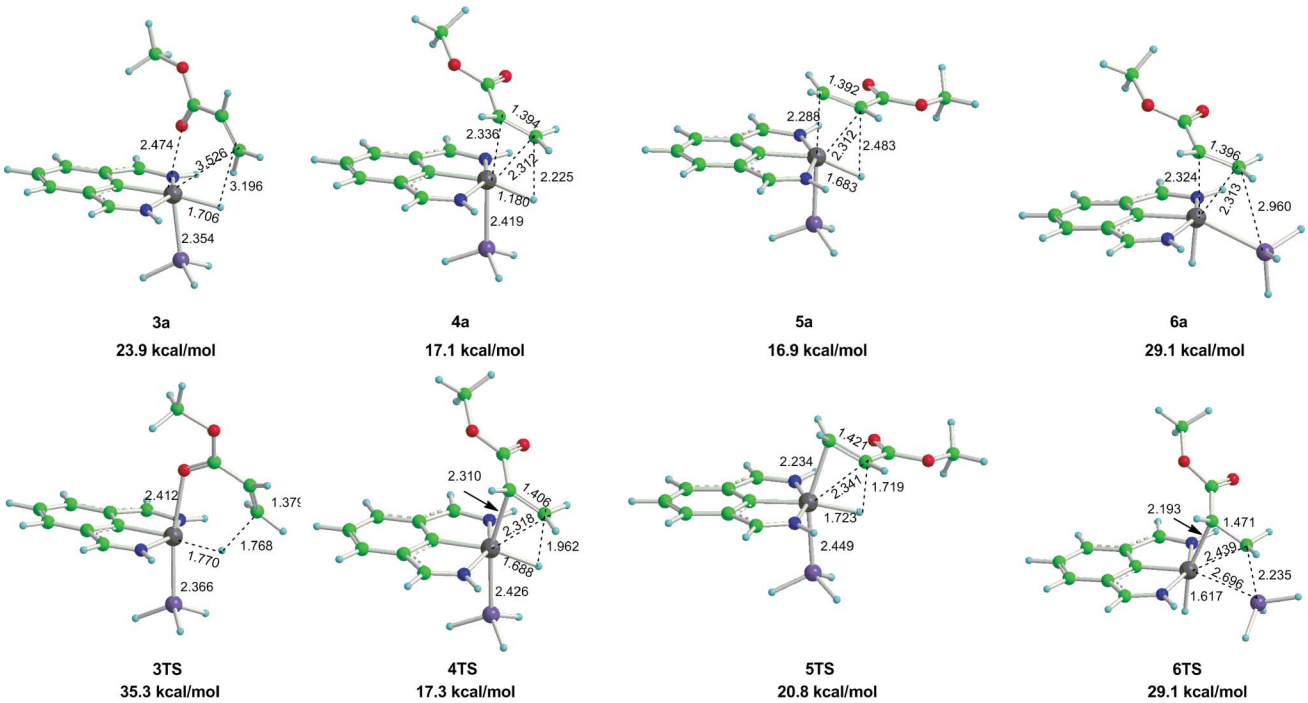

Fig. 2 Optimized geometries of intermediates and transition states in model system; distances are in angstrom (Å).

positive charge and therefore be more attractive to the attacking hydride. Moreover, silyl migration transition state **6TS** lies *ca.* 11.8 kcal mol^{-1} above **4TS**, indicating that hydride is a much better nucleophile than SiH_3 group and its migration to C═C bond occurs more easily with relatively lower barrier. The activation energy of the silyl migration in the present study is about 29.1 kcal mol^{-1}, which is higher than the reported activation energy (18.1 kcal mol^{-1}) of silyl migration to the Rh-coordinated ethylene.[21] Also it is higher than the activation energies of silyl migration to the Ru-coordinated acetylene with and without an HCN ligand, about 22.7 and 19.2 kcal mol^{-1}, respectively.[22] Finally, four corresponding products have been obtained, including O-bound rhodium enolate (**3b**), C-bound rhodium complexes from hydride migration (**4b** and **5b**) and SiH_3 migration (**6b**). The product **4b** is much more stable than the other three products (Fig. 4). Furthermore, it should be noted that in **4b** the Rh–H distance is 2.153 Å and the newly formed C–H bond (1.132 Å) is longer than the usual C–H bond (1.10 Å). These features suggest that a β–H agostic interaction is formed between Rh and the C–H bond,[23] whereas no obvious agostic interaction is found in **3b** and **6b**.

Following the hydride migration, **4b** may isomerize to 18-electron oxa-π-allyl rhodium complex **7a**, which is about 3.2 kcal mol^{-1} higher than **4b**. It is supposed that aldol reaction occurs between **7a** and aldehyde to form **7b** *via* transition state **7TS** with an activation free energy of *ca.* 15 kcal mol^{-1} (Fig. 3). An alternative pathway leading to **4b** from **7b** was also considered (Scheme 3). Such a pathway is relevant in rhodium(I) mediated arylation of aldehydes with arylboronic acids under base and water free conditions.[24] If the aldehyde attacks directly to C-bound rhodium complex **4b**, it must cross a high barrier with about 37 kcal mol^{-1} (**9TS**). The four-membered-ring transition structure **9TS** is so crowded that the acrylate is repulsed and the distance between rhodium and the α-carbon of acrylate is extended to 3.067 Å. From **7b**, reductive elimination is the last step to yield the final product **8** with only a barrier of 5.3 kcal mol^{-1}.

Fig. 4 shows the overall relative free energy profile for different pathways in the model system. The most favorable process in both thermodynamic and kinetic aspects is shown by a solid line. The overall relative free energy profile indicates that hydride migration to the acrylate β-carbon is the rate-determining step

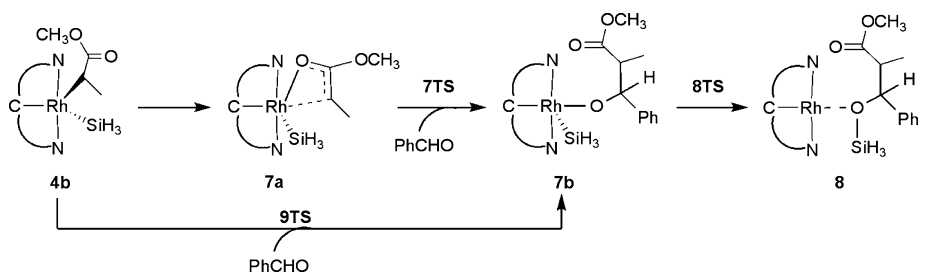

Scheme 3 Aldol reaction and reductive elimination reaction with simplified model system.

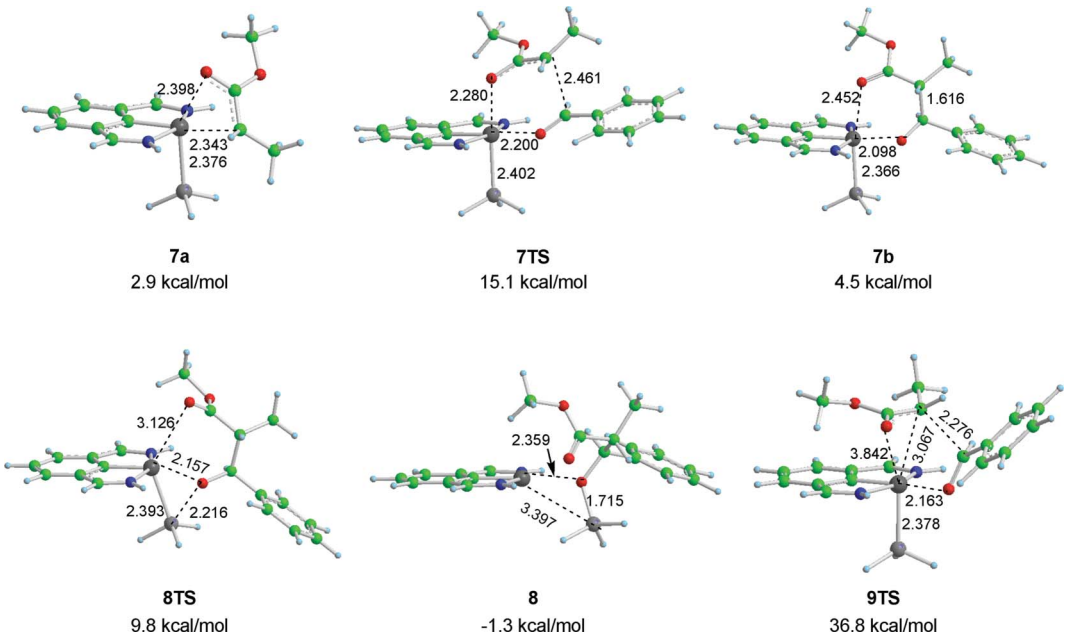

Fig. 3 Optimized geometries of intermediates and transition states in model system; distances are in angstrom (Å).

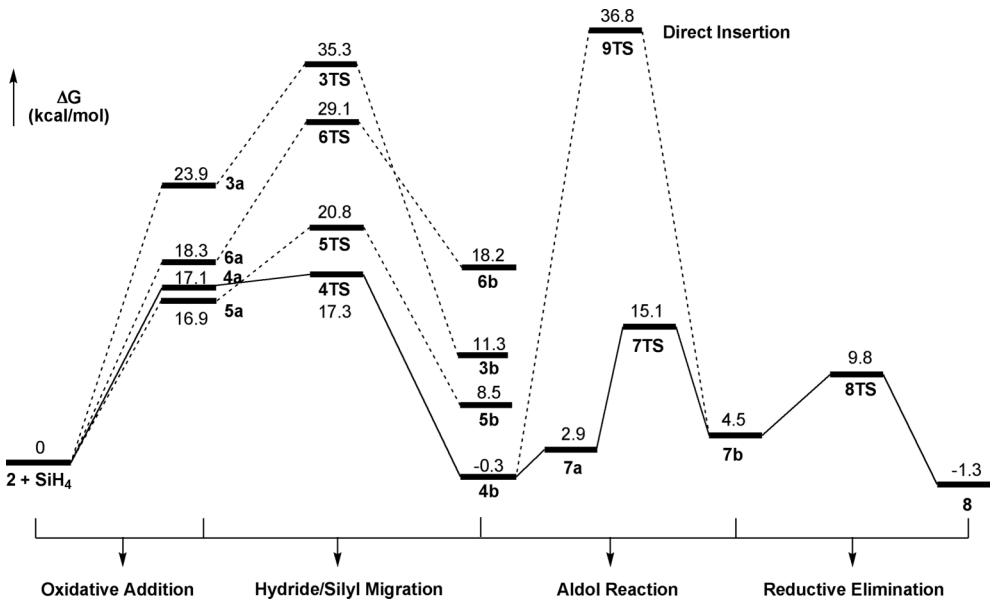

Fig. 4 Calculated relative free energies of the structures shown in Scheme 2 and Scheme 3 for the simplified model system.

(activation energy $\Delta E_a^{\neq}$ of this reaction is ~17.3 kcal mol^{-1}), which has the potential to determine the chirality at C2 (α-carbon). It is supposed that the stereochemistry is controlled in both the hydride migration step and the aldol reaction step. Therefore, we focus on the hydride migration and aldol reaction pathway for the following study.

3 Rh(Phebox-ip) catalyzed reductive aldol reactions

After establishing the key mechanistic aspects, we turned to address the stereochemistry control and asymmetric induction using the real system that includes the hydrosilane (EtO)Me_2SiH, *tert*-butyl acrylate and benzaldehyde with the chiral catalyst Rh(Phebox-ip) (abbreviated as Rh-ip).

3.1 Overall reaction potential energy surface. As shown in Scheme 4 and Fig. 5, similarly to the above model study, the catalytic cycle for the real system proceeds *via* oxidative addition, hydride migration, aldol reaction and reductive elimination. Considering the fact that bulky substituents might influence the barrier of tautomerizations and isomerizations between hydride migration and aldol reaction, these steps have also been investigated in detail. The relative energies of these transition states are calculated to be lower than those of the hydride migration. Therefore, the key conclusion from the model study, *i.e.* that the hydride migration

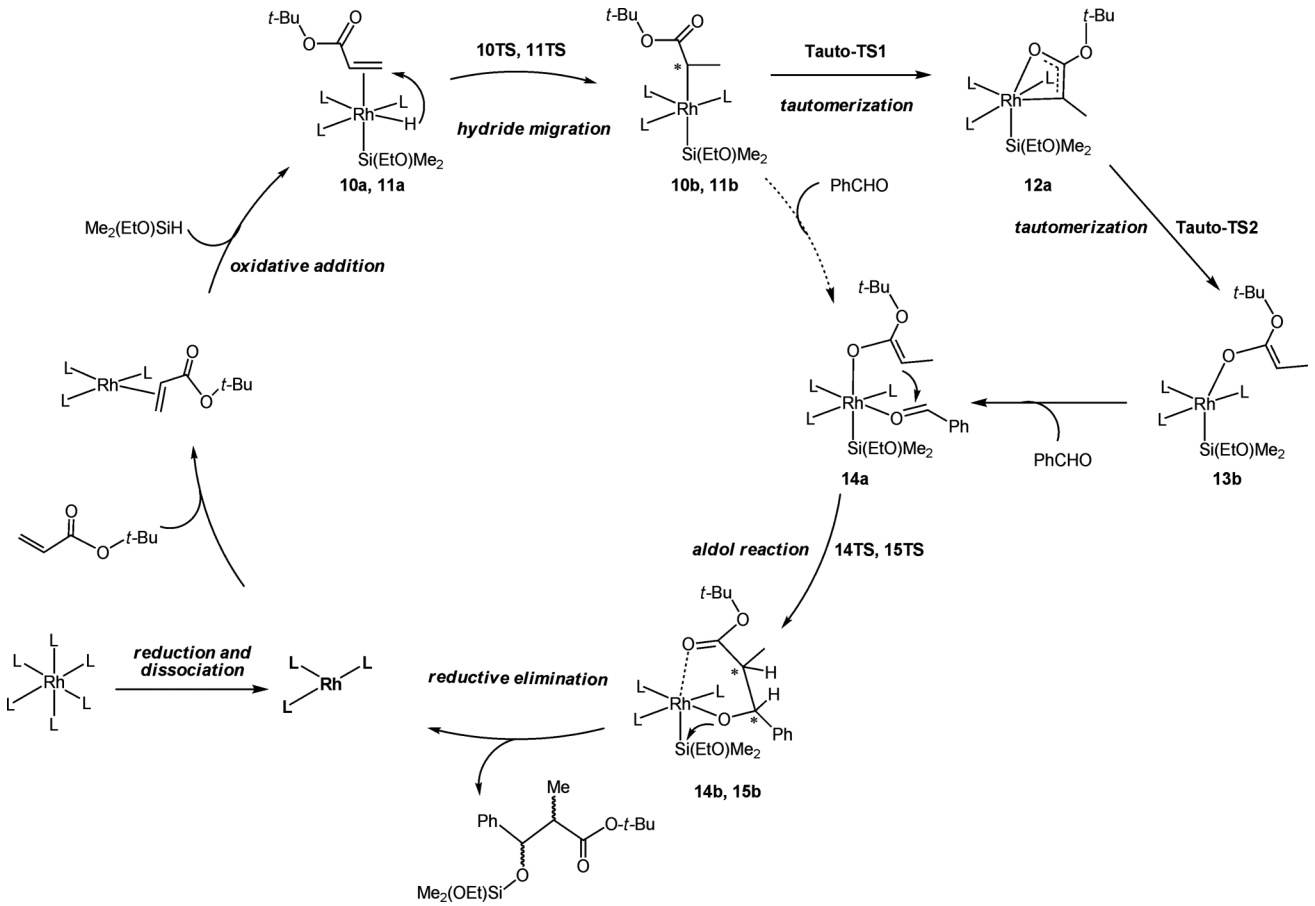

Scheme 4 Reaction pathway of the reductive aldol reaction between benzaldehyde and *tert*-butyl acrylate under Rh(Phebox) catalysis.

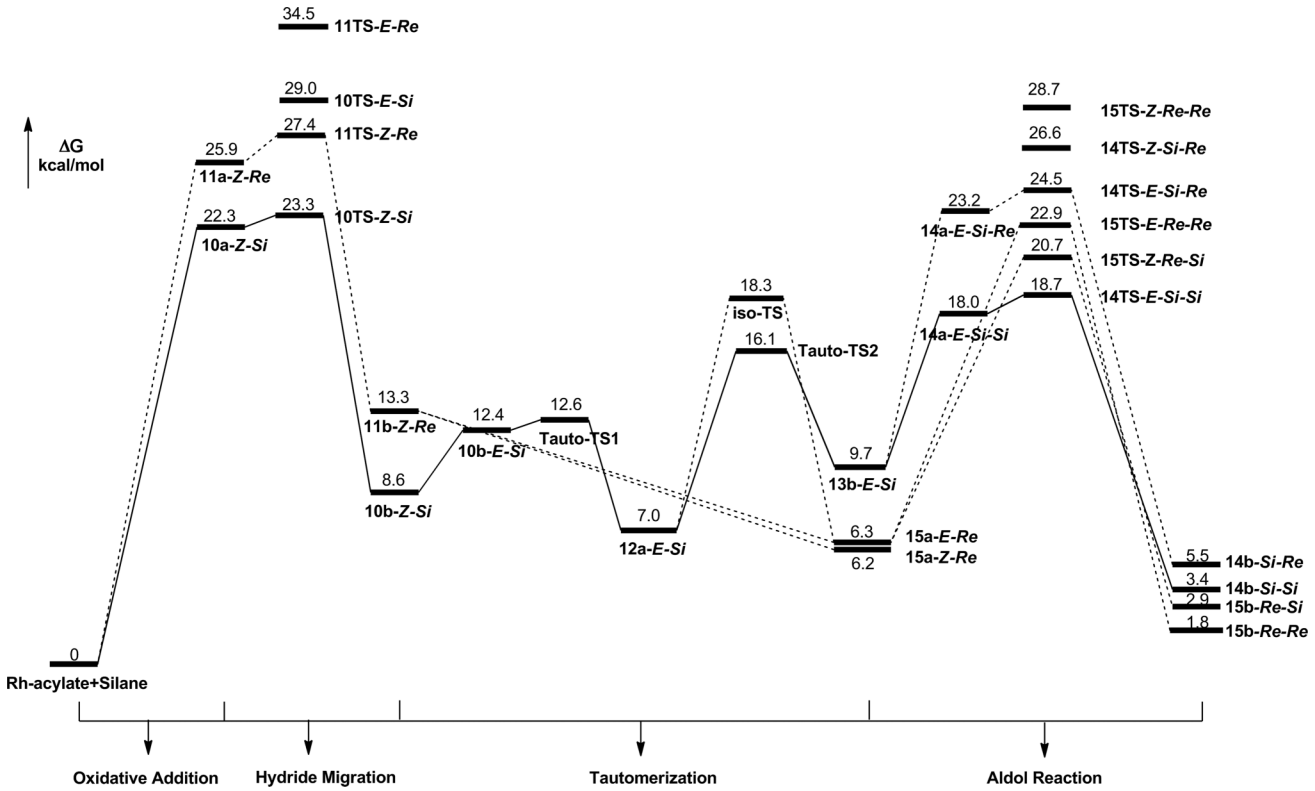

Fig. 5 Calculated free energy profile in the gas phase for the reaction shown in Scheme 4.

is the rate-determining step, still holds true. Furthermore, the enantioselectivity and diastereoselectivity of the reaction are supposed to be determined by both the hydride migration and the aldol reaction. However, here the asymmetric catalyst Rh-ip leads to more transition states (**10TS/11TS** and **14TS/15TS**) which lead to different diastereomers. The most favorable pathway (solid line in Fig. 5) indeed results in the predominant diastereomer obtained in the experiment, indicating that our calculations are reliable. In the following section, we will mainly focus on the origin of the stereoselectivity based on hydride migration and aldol reaction.

3.2 Hydride migration: determination of the chirality of α-C. According to the option of two different faces (*Si* and *Re*) and two different orientations (*Z* and *E*)[25] of the coordinated *tert*-butyl acrylate, in total four transition states are possible (Fig. 6). The C═C bond of *tert*-butyl acrylate is parallel to the Rh–H bond in all cases. The chirality of α-C is determined by the coordination face of the C═C bond. The Rh-bound C═C bond of *tert*-butyl acrylate in **11a-*Z-Re*** has a large steric repulsion with the isopropyl group of the Rh-ip, which causes **11a-*Z-Re*** to be less stable than **10a-*Z-Si*** by about 3.6 kcal mol^{-1} (Figure S1 in the ESI†). Such steric repulsion becomes more severe when the two moieties are closer to each other in the transition state. As a result, the energy difference between the corresponding transition states **10TS-*Z-Si*** and **11TS-*Z-Re*** is larger. The optimized transition structures are depicted in Fig. 6. The Rh–H distance (1.692 Å) in **10TS-*Z-Si*** is almost the same as that (1.693 Å) in **11TS-*Z-Re***, and the distance between the β-carbon atom and H (hydride) are both shortened by about 0.55 Å in the two transition states. The steric repulsion between the isopropyl group of Rh-ip and acrylate makes **11TS-*Z-Re*** less stable than **10TS-*Z-Si*** by about 4.1 kcal mol^{-1} which is consistent with the 3.6 kcal mol^{-1} difference between **10a-*Z-Si*** and **11a-*Z-Re***. We also explored the other two *E*-TSs, **10TS-*E-Si*** and **11TS-*E-Re***, in which the carbonyl group is *trans* to the C═C double. Both of these two TSs have higher energy than those of the *Z*-TSs.

As expected, the energy difference between the two intermediates **10b-*Z-Si*** and **11b-*Z-Re*** is even larger (4.7 kcal mol^{-1}) than those of the two transition states, since the structures are more compact (Fig. 7). Furthermore, an important difference between **10b-*Z-Si*** and **11b-*Z-Re*** is observed in the agostic interaction. In **10b-*Z-Si***, the distance between Rh and H (the hydrogen in the newly formed C–H bond) is 2.163 Å, which is considerably shorter than that of **11b-*Z-Re*** (2.407 Å) (Figure S1 in the ESI†). This clearly indicates that the β-H agostic interaction of **10b-*Z-Si*** is much stronger than **11b-*Z-Re***, which contributes to the stabilization of **10b-*Z-Si***. In a word, the chirality of α-C is determined in the hydride migration step and the pathway leading to **10b-*Z-Si*** is most favorable because of the steric hindrance between the isopropyl group of Rh-ip and *tert*-butyl acrylate.

3.3 Tautomerization and isomerization: relay of stereochemistry. In order to access a structure in which the aldol reaction can occur, the C-enolate intermediate **10b-*Z-Si*** has to tautomerize to an O-enolate intermediate.[26] It is worth pointing out that **10b-*Z-Si*** is a 16-electron structure with a d^6 Rh^{III} center. It has a tendency to isomerize to 18-electron oxa-π-allyl rhodium complex **12a-*E-Si*** (Fig. 8), which is calculated to be more stable than **10b-*Z-Si*** by about 1.6 kcal mol^{-1}. The chirality of α-C in **12a-*E-Si*** is consistent with that of **10b-*Z-Si*** since the facile *Z*/*E* transformation does not change the chirality at α-C and the transition state **Tauto-TS1** retains the π-face. To confirm that the rhodium bound C-enolate (**10b-*Z-Si*** or **10b-*E-Si***) can isomerize to 18-electron oxa-π-allyl rhodium complex **12a-*E-Si***, we made some efforts to locate the exact transition state (**Tauto-TS1**). Our IRC calculation suggests that it really connects **10b-*E-Si*** and **12a-*E-Si***. The structure of

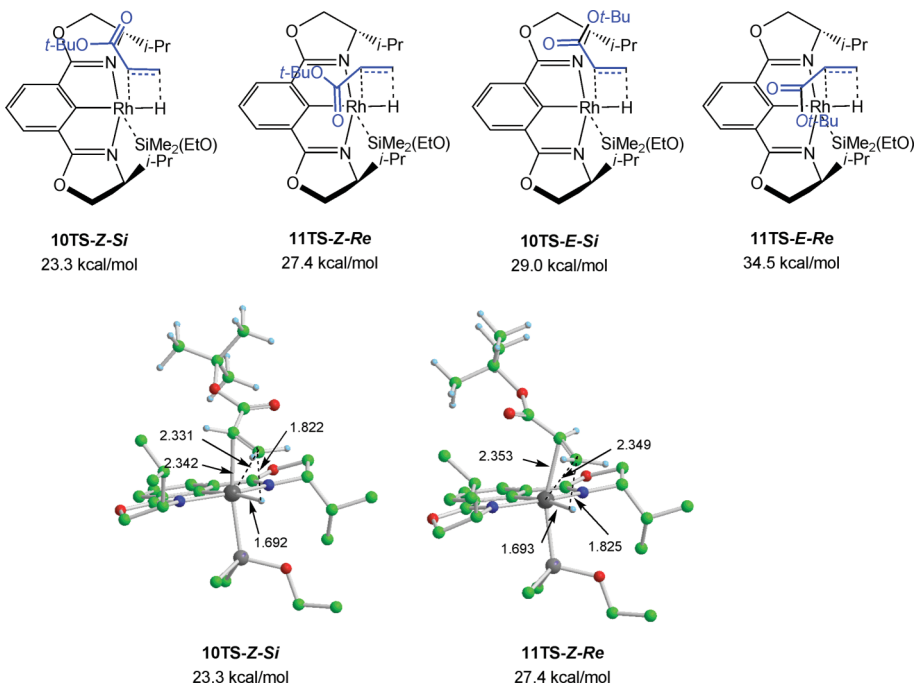

Fig. 6 Optimized transition structures of **10TS** and **11TS**. Hydrogen atoms of Rh(Phebox) are ignored for clarity; distances are in angstrom (Å). ***Z*** and ***E*** indicate the relative position of C═O and C═C of the acrylate.

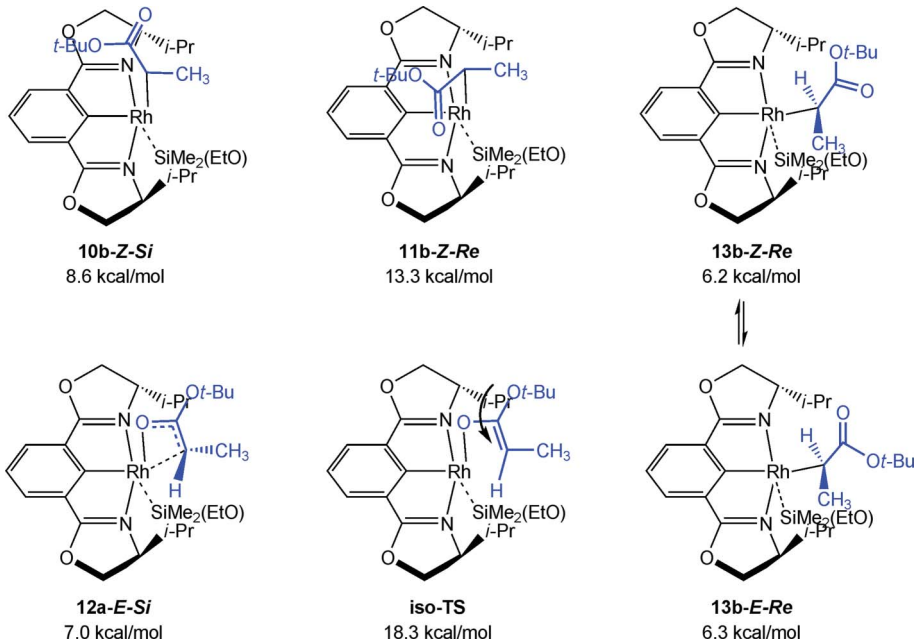

Fig. 7 Structures of **10b**, **11b**, **12a**, **iso-TS** and **13b**.

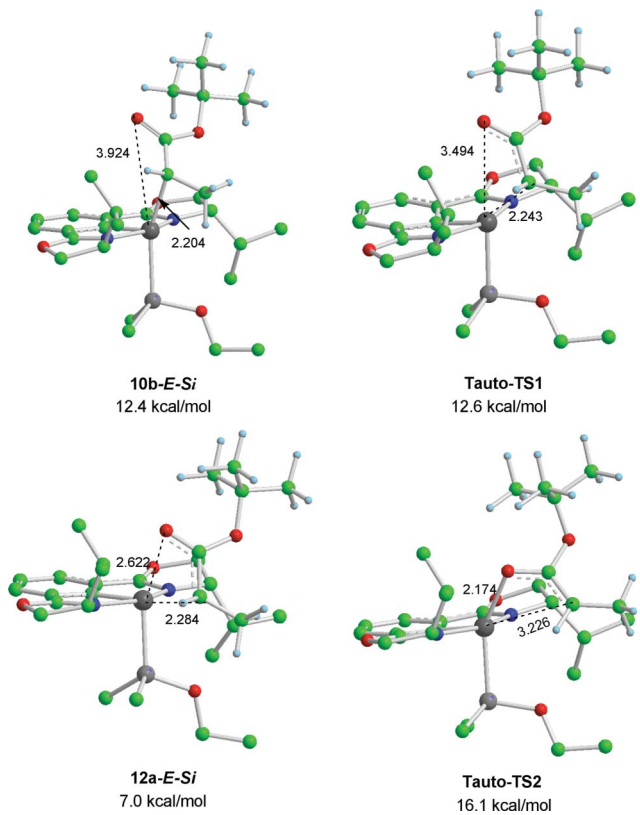

Fig. 8 Optimized geometries of **10b-*E-Si***, **Tauto-TSs** and **12a-*E-Si***. Hydrogen atoms of Rh(Phebox-ip) are ignored for clarity; distances are in angstrom (Å).

Tauto-TS1 has only one imaginary frequency (–25.39). Since this negative eigenvalue is very small, we further scanned the Rh–O distance to find the maximum point (**Tauto-Max1**) (16.5 kcal mol^{-1}) on the energy surface (Figure S2 in the ESI†). Both the **Tauto-TS1** and **Tauto-Max1** suggest that the energy barrier for rhodium bound C-enolate tautomerize to oxa-π-allyl rhodium species is very low.

Lin and Dang have investigated the tautomerization between O- and C-bound enolate of copper(I).[27] Their computations suggest that the C-bound Cu^{I} enolate undergoes a keto-to-enol tautomerization to give an O-bound enolate in the borylation of acrolein but not in the borylation of methacrylate due to the inertness of the ester group. However, it is easy to form oxa-π-allyl species for rhodium.[28] Although the oxa-π-allyl rhodium species (**12a-*E-Si***) is relatively stable, it is required that it tautomerizes to rhodium bound O-enolate and provides a vacant site to trap the benzaldehyde. How easy is it to form the O-enolate species from the hetero-allyl species? Taking this into account, we located the **Tauto-TS2** which is the transition state from oxa-π-allyl complex **12a-*E-Si*** to O-enolate complex **13b-*E-Si*** (Figure S3 in the ESI†). During this process, the chiral α-C in **12a-*E-Si*** was transformed into a sp^2-C in **13b-*E-Si***. In the O-enolate complex **13b-*E-Si***, the Rh-bound O and the methyl group are on the opposite side of the C═C bond. This is a correct starting point for the aldol reaction which results in an *anti*-product. Such a process can be regarded as a relay of stereochemistry from **10b-*Z-Si*** to **13b-*E-Si***.

Although the above pathway leads to **13b-*E-Si*** smoothly, we wondered whether the chirality at the α-C of Rh oxa-π-allyl **12a-*E-Si*** may be lost in an isomerization to the *Re*-facial intermediate. Transition state **iso-TS** (Fig. 7) has been located with a relative energy of about 18.3 kcal mol^{-1}. The barrier is higher than **Tauto-TS2** and comparable to those of aldol reactions,[29] implying that such an isomerization process is unlikely to take place. Nevertheless, to ensure a more complete space is covered, we still take **13b-*E-Re*** into consideration in the following aldol reaction step.

3.4 Aldol reaction: determination of diastereoselectivity. In the aldol reaction step, by combining three variables, *i.e.* *Z*/*E*

configuration of the Rh-enolate, *Si*/*Re*-face of the Rh-enolate, and *Si*/*Re*-face of benzaldehyde, there are eight transition states to be considered. Many efforts have been taken to locate these transition states. The stereoviews of the four most stable transition states **14TS-*E-Si-Si***, **14TS-*E-Si-Re***, **15TS-*Z-Re-Si*** and **15TS-*E-Re-Re*** are shown in Fig. 9. The transition states **14TS-*Z-Si-Re*** and **15TS-*Z-Re-Re***, which are relatively less stable, were also found (Figure S4 in the ESI†). The other two structures **14TS-*Z-Si-Si*** and **15TS-*Re-Si*** could not be located due to the apparent repulsion between the substrate and the catalyst, indicating that these two transition states, if they exist, are very unstable and can be excluded from consideration. The energetic and structural differences between the transition state **14TS-*E-Si-Si*** and the corresponding aldehyde complex **14a-*E-Si-Si*** (Figure S4 in the ESI†) are small, indicating that **14TS-*E-Si-Si*** is a very early transition state. The situation for the **14TS-*E-Si-Re*/14a-*E-Si-Re*** couple is similar. Such low barriers are understandable because the Rh center activates both the enolate and the benzaldehyde. This implies that the aldol reaction is ready to occur when benzaldehyde approaches the Rh-enolate in the correct fashion. In all of the transition states located, benzaldehyde coordinates to the Rh on the same equatorial plane with Phebox-ip, while enolate occupies the apical position which is less sterically demanding. The diastereoselectivity, *i.e.* energy difference between different transition states, is mostly caused by the steric repulsion between Phebox-ip and enolate or benzaldehyde. The two isopropyl groups of the Phebox-ip control different stereochemistry. **14TS-*E-Si-Si*** adopts a chair-like structure which is free of steric congestion. Neither the *tert*-butyl group of the enolate nor the phenyl group of the aldehyde suffers repulsion from the isopropyl groups. Thit makes **14TS-*E-Si-Si*** the most stable one among all the transition states for the aldol reactions. This transition state results in an *anti*-(2*R*,3*S*) product, which was observed as the predominant diastereomer in the experiment.[10] The benzaldehyde in **14TS-*E-Si-Re*** accesses the Rh-enolate moiety with its *Re* face. To avoid the repulsion from the isopropyl group of the catalyst, the phenyl group of benzaldehyde has to take a different orientation with that in **14TS-*E-Si-Si***. As a result, **14TS-*E-Si-Re*** adopts a boat-like structure.

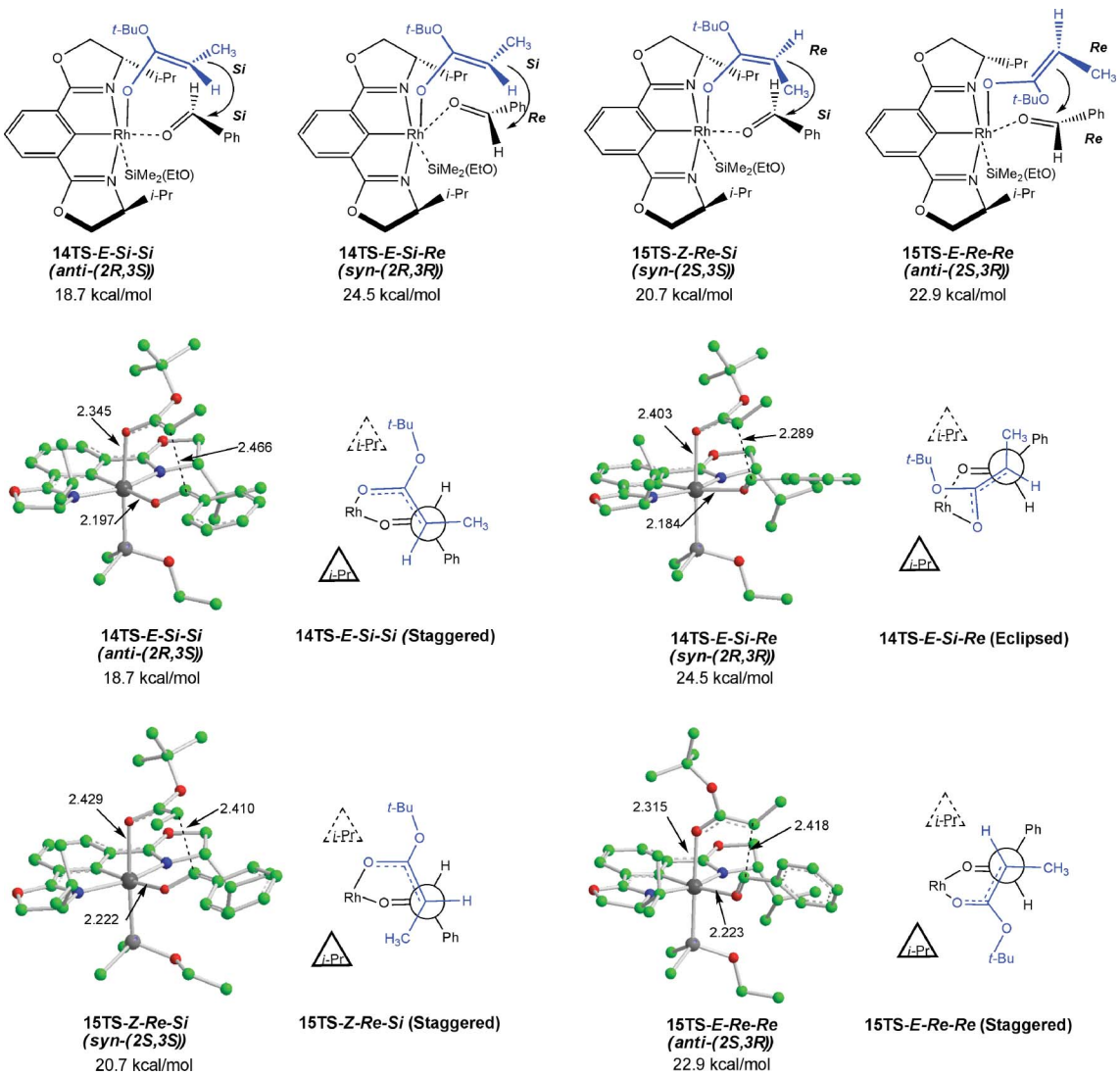

Fig. 9 Four most stable transition structures of **14TSs** and **15TSs** in different approaching pathways, and Newman projections of the transition states along the optimized geometries. Some hydrogen atoms are ignored for clarity and distances are in angstrom (Å).

The distortion from such an eclipsed conformation makes **14TS-*E-Si-Re*** less stable than **14TS-*E-Si-Si*** by *ca.* 5.8 kcal mol^{-1}. The same orientation of benzaldehyde can also be found in **15TS-*E-Re-Re***. However, in this case, the strain is partly reduced because the enolate moiety also renders its *Re* face to achieve a chair-like conformation. The most stable transition state for the *Z*-enolate is **15TS-*Z-Re-Si***, which lies 2 kcal mol^{-1} higher in free energy than its *E*-enolate counterpart **14TS-*E-Si-Si***. In other words, the pathway leading to the *syn*-(2*S*,3*S*) product is anyway unfavorable in the steps of both hydride migration and aldol reaction. Overall, our calculation is in line with experiment in predicting *anti*-(2*R*,3*S*) as the major product with high enantioselectivity. More importantly, the transition structures illustrate the origin of the high diastereoselectivity.

Conclusions

The mechanism of Rh(Phebox-ip) catalyzed asymmetric reductive aldol reaction of benzaldehyde and *tert*-butyl acrylate with hydrosilane has been investigated by the density functional theory method of B3LYP. Several different pathways have been explored. The most favorable pathway involves five steps: oxidative addition, hydride migration to the α-C of acrylate, tautomerization from rhodium bound C-enolate to rhodium bound O-enolate, aldol reaction with benzaldehyde, and reductive elimination. The hydride migration and the aldol reaction are the two crucial reaction steps in the catalytic cycle. The hydride migration is found to be the rate-determining step with an activation barrier of 23.3 kcal mol^{-1} for the real system. This step also determines the chirality at C2. The *anti*-(2*R*,3*S*) product is calculated to be formed from the most favorable pathway *via* the transition state **14TS-*E-Si-Si*** for aldol reaction. The results are in good agreement with previous experiments. Furthermore, the transition structures demonstrate that the stereoselectivity is mainly attributed to the steric repulsion from the two isopropyl groups of the Phebox-ip. This provides a foundation for the understanding of the recent report by Nishiyama *et al.* on the reductive aldol reaction of enone with aromatic aldehyde, which gives *anti* product but with opposite enantioselectivity from the current case.[30] Further study will also direct the design of new catalysts.

Acknowledgements

We are grateful to the National Science Foundation of China (20225312), Peking University Shenzhen Graduate School (grant to JM Quan), and the Shenzhen municipal "Shuang Bai Project" for financial support of this research.

Notes and references

1 (*a*) R. Noyori, *Asymmetric Catalysis in Organic Synthesis*, Wiley, New York, 1994; (*b*) I. P. Beletskaya and A. V. Cheprakov, *Chem. Rev.*, 2000, **100**, 3009; (*c*) N. Miyaura and A. Suzuki, *Chem. Rev.*, 1995, **95**, 2457; (*d*) A. Suzuki, *J. Organomet. Chem.*, 1999, **576**, 147.
2 (*a*) M. Shibasaki, H. Sasai and T. Arai, *Angew. Chem.*, 1997, **109**, 1290; (*b*) C. X. Zhao, M. O. Duffey, S. J. Taylor and J. P. Morken, *Org. Lett.*, 2001, **3**, 1829; (*c*) I. Shibata, H. Kato and A. Baba, *Angew. Chem., Int. Ed.*, 2004, **43**, 711; (*d*) S. E. Denmark, J. R. Jr. Heemstra and G. L. Beutner, *Angew. Chem., Int. Ed.*, 2005, **44**, 4682; (*e*) O. Chuzel, J. Deschamp, C. Chausteur and O. Riant, *Org. Lett.*, 2006, **8**, 5943; (*f*) M. Sugiura, N. Sato, S. Kotani and M. Nakajima, *Chem. Commun.*, 2008, 4309; (*g*) L. M. Geary and P. G. Hultin, *Tetrahedron: Asymmetry*, 2009, **20**, 131.
3 (*a*) S. Sakuma, M. Sakai, R. Itooka and N. Miyaura, *J. Org. Chem.*, 2000, **65**, 5951; (*b*) N. Jiao, L.-W. Ye and S.-M. Ma, *Chin. J. Org. Chem.*, 2004, **24**, 472; (*c*) Y. Otomaru, K. Okamoto, R. Shintani and T. Hayashi, *J. Org. Chem.*, 2005, **70**, 2503; (*d*) C. Navarro, A. Moreno and A. G. Csákÿ, *J. Org. Chem.*, 2009, **74**, 466; (*e*) H. J. Edwards, J. D. Hargrave, S. D. Penrose and C. G. Frost, *Chem. Soc. Rev.*, 2010, **39**, 2093.
4 (*a*) T. Naota, H. Taki and S. I. Murahashi, *J. Am. Chem. Soc.*, 1989, **111**, 5954; (*b*) S. Isayama and I. Mukaiyama, *Chem. Lett.*, 1989, 2005; (*c*) S. Kiyooka, A. Shimizu and S. Torii, *Tetrahedron Lett.*, 1998, **39**, 5237; (*d*) T. Ooi, K. Doda, D. Sakai and K. Maruoka, *Tetrahedron Lett.*, 1999, **40**, 2133.
5 A. Revis and T. K. Hilty, *Tetrahedron Lett.*, 1987, **28**, 4809.
6 (*a*) G. A. Marriner, S. A. Ganer and M. J. Krische, *J. Org. Chem.*, 2004, **69**, 1380; (*b*) M. Freiria, A. J. Whitehead and W. B. Mortherwell, *Tetrahedron*, 2004, **60**, 2673; (*c*) H. Y. Jang, R. R. Huddleston and M. J. Krische, *J. Am. Chem. Soc.*, 2002, **124**, 15156; (*d*) H. W. Lam and P. M. Joensuu, *Org. Lett.*, 2001, **3**, 1901; (*e*) L. C. Wang, H. Y. Jang and M. J. Krische, *J. Am. Chem. Soc.*, 2002, **124**, 9448; (*f*) N. O. Fuller and J. P. Morken, *Org. Lett.*, 2005, **7**, 4867; (*g*) D. Zhao, K. Oisaki, M. Kanai and M. Shibasaki, *J. Am. Chem. Soc.*, 2006, **128**, 14440.
7 (*a*) A. E. Russell, N. O. Fuller and J. P. Morken, *Org. Lett.*, 2004, **6**, 2309; (*b*) I. Shibata, H. Kato and A. Baba, *Angew. Chem.*, 2004, **116**, 729.
8 C. C. Christa and M. John, *Org. Lett.*, 2007, **9**, 537.
9 (*a*) Y. Motoyama and H. Nishiyama, *Organometallics*, 2001, **20**, 1580; (*b*) Y. Motoyama and H. Nishiyama, *Organometallics*, 2002, **21**, 3408; (*c*) T. Shiomi, J.-I. Ito, Y. Yamamoto and H. Nishiyama, *Eur. J. Org. Chem.*, 2006, 5594; H. Nishiyama and J.-I. Ito, *Chem. Commun.*, 2010, **46**, 203.
10 H. Nishiyama, T. Shiomi, Y. Tsuchiya and I. Matsuda, *J. Am. Chem. Soc.*, 2005, **127**, 6972.
11 (*a*) P.-O. Norrby and G. C. Lloyd-Jones, *J. Mol. Catal. A: Chem.*, 2010, **324**, 1; (*b*) H.-J. Wang, J. Shi, M. Fang, Z. Li and Q.-X. Guo, *J. Phys. Org. Chem.*, 2010, **23**, 75.
12 M. J. Frisch, G. W. Trucks, H. B. Schlegel, G. E. Scuseria, M. A. Robb, J. R. Cheeseman, J. A. Montgomery, Jr., T. Vreven, K. N. Kudin, J. C. Burant, J. M. Millam, S. S. Iyengar, J. Tomasi, V. Barone, B. Mennucci, M. Cossi, G. Scalmani, N. Rega, G. A. Petersson, H. Nakatsuji, M. Hada, M. Ehara, K. Toyota, R. Fukuda, J. Hasegawa, M. Ishida, T. Nakajima, Y. Honda, O. Kitao, H. Nakai, M. Klene, X. Li, J. E. Knox, H. P. Hratchian, J. B. Cross, V. Bakken, C. Adamo, J. Jaramillo, R. Gomperts, R. E. Stratmann, O. Yazyev, A. J. Austin, R. Cammi, C. Pomelli, J. W. Ochterski, P. Y. Ayala, K. Morokuma, G. A. Voth, P. Salvador, J. J. Dannenberg, V. G. Zakrzewski, S. Dapprich, A. D. Daniels, M. C. Strain, O. Farkas, D. K. Malick, A. D. Rabuck, K. Raghavachari, J. B. Foresman, J. V. Ortiz, Q. Cui, A. G. Baboul, S. Clifford, J. Cioslowski, B. B. Stefanov, G. Liu, A. Liashenko, P. Piskorz, I. Komaromi, R. L. Martin, D. J. Fox, T. Keith, M. A. Al-Laham, C. Y. Peng, A. Nanayakkara, M. Challacombe, P. M. W. Gill, B. Johnson, W. Chen, M. W. Wong, C. Gonzalez, and J. A. Pople, *Gaussian 03, Revision D.01*, Gaussian, Inc, Wallingford CT, 2004.
13 (*a*) A. D. Becke, *J. Chem. Phys.*, 1993, **98**, 5648; (*b*) C. Lee, W. Yang and R. G. Parr, *Phys. Rev. B*, 1988, **37**, 785; (*c*) A. D. Becke, *J. Chem. Phys.*, 1993, **98**, 1372; (*d*) P. J. Stephens, F. J. Devlin, C. F. Chabalowski and M. J. Frisch, *J. Phys. Chem.*, 1994, **98**, 1623; (*e*) W. J. Hehre, L. Radom, P. V. Schleyer, and J. A. Pople, *Ab initio Molecular Orbital Theory*, Wiley, New York, 1986.
14 (*a*) R. Ditchfiled, W. J. Hehre and J. A. Pople, *J. Chem. Phys.*, 1971, **54**, 724; (*b*) W. J. Hehre, R. Ditchfiled and J. A. Pople, *J. Chem. Phys.*, 1972, **54**, 2257; (*c*) P. C. Hariharan and J. A. Pople, *Theor. Chim. Acta*, 1973, **28**, 213.
15 (*a*) P. J. Hay and W. R. Wadt, *J. Chem. Phys.*, 1985, **82**, 270; (*b*) W. R. Wadt and P. J. Hay, *J. Chem. Phys.*, 1985, **82**, 284.
16 (*a*) K. Fukui, *J. Phys. Chem.*, 1970, **74**, 4161; (*b*) K. Fukui, *Acc. Chem. Res.*, 1981, **14**, 363.
17 S. Miertus, E. Scrocco and J. Tomasi, *Chem. Phys.*, 1981, **55**, 117.
18 Y. Kanazawa and H. Nishiyama, *Chem.–Eur. J.*, 2006, **12**, 63.
19 (*a*) M. A. Schroeder and M. S. Wrighton, *J. Organomet. Chem.*, 1977, **128**, 345; (*b*) A. Millan, E. Towns and P. M. Maitlis, *J. Chem. Soc., Chem. Commun.*, 1981, **14**, 673; (*c*) I. Ojima, T. Fuchikami and M. Yatabe, *J. Organomet. Chem.*, 1984, **260**, 335; (*d*) C. L. Randolph and M. S. Wrighton, *J. Am. Chem. Soc.*, 1986, **108**, 3366; (*e*) A. J. Chalk

and J. F. Harrod, *J. Am. Chem. Soc.*, 1965, **87**, 16; (*f*) Y. Nishibayashi, K. Segawa, K. Ohe and S. Uemura, *Organometallics*, 1995, **14**, 5486; (*g*) D. A. Evans, F. E. Michael, J. S. Tedrow and K. R. Campos, *J. Am. Chem. Soc.*, 2003, **125**, 3534.
20 (*a*) Z. Lin and M. B. Hall, *Inorg. Chem.*, 1991, **30**, 646; (*b*) B. J. Coe and S. J. Glenright, *Coord. Chem. Rev.*, 2000, **203**, 5; (*c*) L. W. Chung, H. G. Lee, Z. Lin and Y.-D. Wu, *J. Org. Chem.*, 2006, **71**, 6000.
21 (*a*) S. Sakaki, M. Sumimoto, M. Fukuhara, M. Sugimoto, H. Fujimoto and S. Matsuzaki, *Organometallics*, 2002, **21**, 3788; (*b*) S. Sakaki, N. Mizoe and M. Sugimoto, *Organometallics*, 1998, **17**, 2510.
22 L. W. Chung, Y.-D. Wu, B. M. Trost and Z. T. Ball, *J. Am. Chem. Soc.*, 2003, **125**, 11578.
23 (*a*) M. Brookhart, M. L. Green and G. Parkin, *Proc. Natl. Acad. Sci. U. S. A.*, 2007, **104**, 6908; (*b*) M. Etienne, J. E. McGrady and F. Maseras, *Coord. Chem. Rev.*, 2009, **253**, 635.
24 A. I. O. Suarez, J. N. H. Reek and B. de Bruin, *J. Mol. Catal. A: Chem.*, 2010, **324**, 24.
25 The notations *Z* and *E* are used to distinguish the two orientations of carbonyl. *Z* means the carbonyl is *cis* to the C═C bond, while *E* means the other orientation.
26 Similarly to 9TS in Scheme 3, the pathway where the C-enolate species reacts directly with the rhodium bound aldehyde is by far the most unfavorable. See the ESI† for details.
27 L. Dang and Z. Lin, *Organometallics*, 2008, **27**, 4443.
28 T. Hayashi, M. Takahashi, Y. Takaya and M. Ogasawara, *J. Am. Chem. Soc.*, 2002, **124**, 5052.
29 Since without solvent effects the calculations in gas phase overestimate the activation free energies for the aldol reaction due to overestimation of the entropy loss for the bimolecular reaction, see: (*a*) D. H. Wertz, *J. Am. Chem. Soc.*, 1980, **102**, 5316; (*b*) B. O. Leung, D. L. Reid, D. A. Armstrong and A. Rauk, *J. Phys. Chem. A*, 2004, **108**, 2720.
30 T. Shiomi, T. Adachi, J. Ito and H. Nishiyama, *Org. Lett.*, 2009, **11**, 1011.